Hindawi
Journal of Chemistry
Volume 2020, Article ID 3932715, 13 pages
https://doi.org/10.1155/2020/3932715

Research Article

TiO_2 Nanoparticles Decorated Graphene Nanoribbons for Voltammetric Determination of an Anti-HIV Drug Nevirapine

Daniel Apath, Mambo Moyo, and Munyaradzi Shumba

Sensor Lab Research Group, Department of Chemical Technology, Midlands State University, Private Bag 9055 Senga, Gweru, Zimbabwe

Correspondence should be addressed to Mambo Moyo; moyom@staff.msu.ac.zw

Received 17 July 2019; Revised 13 January 2020; Accepted 13 February 2020; Published 26 March 2020

Academic Editor: Mehrab Mehrvar

In the present study, electrochemical behavior of nevirapine on a glassy carbon electrode (GCE) modified with TiO_2 nanoparticles decorated graphene nanoribbons was investigated. Characterization of different components used for modifications was achieved using Fourier transform infrared spectroscopy (FT-IR) and scanning electron microscopy (SEM). The electrochemical behavior of nevirapine on the modified electrodes was examined using cyclic voltammetry (CV), electrochemical impedance spectroscopy (EIS), chronoamperometry (CA), and differential pulse voltammetry (DPV). A considerable oxidation potential decrease of +352 mV for nevirapine in 0.1 M phosphate-buffered saline (PBS), pH 11.0, was achieved due to synergy offered by graphene nanoribbons and TiO_2 compared to graphene nanoribbons (+252 mV) and TiO_2 (−37 mV), all with respect to the glassy carbon electrode. Under optimized conditions, DPV gave linear calibrations over the range of 0.020–0.14 μM. The detection limit was calculated as 0.043 μM. The developed sensor was used for determination of nevirapine in a pharmaceutical formulation successfully.

1. Introduction

The need for reliable, fast, cheap sensing devices for monitoring biomolecules is important in everyday life. Nevirapine (NVP) (11-cyclopropyl-4-methyl-5, 11-dihydro-6H-dipyrido [3,2-b:2′,3′-e] [1, 2] diazepin-6-one) is a non-nucleoside reverse transcriptase inhibitor. Its uses have been highlighted [1, 3]. The continued use of nevirapine in treatment and management of HIV/AIDS in the health sector thus calls for a great need to improve on its reported analytical work. Several analytical methods, such as reversed phase high-performance liquid chromatography (RP-HPLC) [4] and capillary electrophoresis [2], have been used for quantifying NVP in pharmaceutical combinations and some real samples. The growing demand for NVP biomolecule stimulates a search for new and even more effective monitoring techniques, which give better insight on their reported analytical work. Therefore, it is appropriate to develop new and/or improve on the existing analytical techniques regarding their qualitative and quantitative determination in various matrices, namely, human serum, urine, breast milk, and pharmaceutical formulations. The development of sensors with high sensitivity to promote safety and efficiency during administration to patients who depend on these different biomolecules for life support is important. For example, nevirapine in HIV patients' treatment can coexist together with other biomolecules; hence, simultaneous determination is critical, helping management of antiretroviral treatment by minimizing drug-food interactions. Furthermore, nevirapine is also easily oxidized; hence development of an electrochemical sensor is significant.

Electrochemical techniques based on modification of electrode surfaces can grant some remarkable advantages on applications due to provision of high selectivity and improved sensitivity and stability [5–7]. Among the various modifiers, those based on carbon nanomaterials have been shown to be highly promising in electrochemical sensing [8, 9]. In recent years, graphene nanoribbons (GNRs), a one-dimensional form of graphene strip, have shown promising application in fabrication of composites, batteries, supercapacitors, and fuel cells as shown by a high length-to-width ratio, intrinsic energy band gap, and straight edges, availability of larger surface area, and higher electrical conductivity [10–12]. The electron confinement in GNRs has been reported to offer good electronic properties, hence transforming semimetallic to semiconducting properties [13]. Interestingly, GNRs' attractiveness in a variety of electrochemical applications is owed to their outstanding electronic, catalytic, charge transport and surface passivation properties in sensing various organic and inorganic compounds [14, 15]. Oxygen functionalities at the edges of nanoribbons after synthesis reportedly offer homogeneous distribution of metal oxide nanoparticles on the surface of carbon [16].

Metallic oxide nanoparticles have been reported to show favorable properties in electrocatalysis [17, 18]. In this regard, metal oxide nanoparticles such as TiO_2 have been used in sensor fabrication [19–22] due to low cost, nontoxicity, large surface area, biocompatibility, strong adsorptive ability, high uniformity, and excellent catalytic activity [22]. Based on the aforementioned properties, the hybridization of GNRs with metal oxide nanoparticles can provide nanocomposite with synergic properties [23].

In the present study, we have fabricated a simple, cheap glassy carbon electrode (GCE) modified with TiO_2/GNRs as an electrochemical sensor for nevirapine. In our investigation, the atypical properties of GNRs as a good support for making nanoparticle dispersions caused by large surface area, high electrical conductivity, and electrochemical stability in acidic and alkaline electrolytes were an attractive factor. Based on the attractive properties of GNRs and TiO_2, synthesis of TiO_2, GNRs, and a TiO_2/GNRs nanocomposite through environmental friendly methods was carried out. The results showed that the developed sensor had good performances such good reproducibility and good selectivity, owing to the synergic effects of catalysis characters of TiO_2 and GNRs. Besides, to evaluate the applicability of the proposed sensor, it was used to determine nevirapine quantities in a pharmaceutical sample.

2. Experimental

2.1. Chemicals and Solutions. All chemicals used were of analytical grade. Phosphate-buffered saline (PBS) solutions (as supporting electrolyte) with different pH values (6–12) were prepared by mixing standard stock solutions of 0.10 M Na_2HPO_4 and 0.10 M NaH_2PO_4. $NaNO_3$, $K_3Fe(CN)_6$, $K_4Fe(CN)_6$, *N,N*-dimethylformamide (DMF), D (+) glucose monohydrate, 5% nitric acid, nevirapine, 98% H_2SO_4, $KMnO_4$, 30% H_2O_2, and MWCNT (purity of 95%, diameter~20–40 nm, and length~5–15 μm) were obtained from Sigma-Aldrich (South Africa). Titanium acetate dihydrate $[Ti(O_2CCH_3)_2(H_2O)_2]$ and ethanol (C_2H_5OH) were obtained from Associated Chemical Enterprises (South Africa). All solutions were prepared using ultra-Millipore water from Milli-Q Water Systems (Millipore Corp., Bedford, MA, USA). The MWCNTs were purified to remove metal oxide catalysts as reported [18]. The stock solution of appropriate solution of nevirapine was prepared by weighing and dissolving the drug in a 1 : 1 mixture of distilled water and ethanol. The working solutions were prepared by dilution of the stock standard solution with PBS (0.1 M, pH 11). A solution of glucose was prepared by dissolving appropriate amount of glucose in ultrapure water and left for 24 h for mutarotation at room temperature.

2.2. Equipment. Fourier transform infrared spectroscopy (FT-IR, Nicolet 6700 model) was used in IR characterization. The scanning electron microscopy (SEM) image was obtained using a TESCAN Vega TS 5136LM Electron microscope. Cyclic voltammetry (CV), electrochemical impedance spectroscopy (EIS), chronoamperometry, and differential pulse voltammetry (DPV) were performed using an Autolab potentiostat PGSTAT 302N (Eco Chemie, Utrecht, Netherlands) equipped with NOVA 1.10 software. Sonicator model KQ-250B was used for agitation of samples. The pH of the solutions was measured and adjusted by a Thermo Scientific Orion Star A211 pH meter.

2.3. Preparation of Graphene Nanoribbons. Graphene nanoribbons (GNRs) were prepared as described in literature with some little modifications [24, 25]. Briefly, a suspension was formed by dissolving 100 mg of MWCNT in 3.4 mL of 98% H_2SO_4 and then homogenized via ultrasonication for 1 h. Thereafter, the suspension solution was placed in an ice bath accompanied with vigorous stirring and 75 mg of $NaNO_3$ was then added. Next, 450 mg of $KMnO_4$ was added to the suspension. Upon completion of reaction, 20 mL of 5% sulphuric acid solution was added and reaction allowed to cool. As soon as bubble formation started, 2 mL of 30% H_2O_2 was added dropwise. After approximately 30 min, centrifugation and washing with 5% nitric acid three times and deionized water five times were carried out followed by filtration and drying in an oven at 90°C for 12 h under vacuum. The prepared GNRs were ascertained to contain oxygen-containing functional groups.

2.4. Preparation of TiO_2 Nanoparticles. The sol-gel process was used for the synthesis of TiO_2 nanoparticles at 80–90°C. Briefly, 2.195 g of titanium acetate dihydrate was dissolved in 100 mL ethanol followed by stirring in ambient atmosphere. 1.122 g KOH was dissolved in 10 mL distilled water and then added to the titanium acetate dihydrate-ethanol solution dropwise under continuous stirring. The mixed solution turned into a jelly form and a milky white solution was obtained after a few minutes. Furthermore, the mixture was then heated for 3 h at 80–90°C without stirring. Centrifugation was applied to the resulting suspension to obtain intended product. Finally, the mixture was washed with ultra-Millipore water in an ultrasonic bath and then the powder dried at 70°C overnight.

2.5. Preparation of TiO_2/GNR and TiO_2/GNR/GCE. The suspension of TiO_2 (1 mg/mL) was added to GNRs (2 mg/mL) DMF solution (1 : 2) and sonicated for 4 h at room temperature to obtain the TiO_2/GNR nanocomposite homogeneous suspension. The GCE was polished to a mirror finish with alumina slurry (0.3 μm). The electrode was sonicated in Millipore water for 5 min during the three successive cleaning stages and finally dried in a stream of nitrogen. The drop dry technique was employed for electrode modification. The optimized volume of the composite, 5 μL of TiO_2/GNR suspension, was drop-casted on the surface of GCE and dried in the oven to obtain TiO_2/GNRs/GCE. The fabrication procedure of the electrochemical sensor is shown in Scheme 1.

2.6. Assay of Nevirapine Tablets. Five nevirapine tablets (each containing 200 mg per tablet) were obtained from local commercial sources. The drugs were crushed to obtain a finely homogenized powder using the mortar. A portion of the powder suitable to prepare 1 mM was weighed and transferred into a 10 mL volumetric flask containing water, sonicated to allow dissolution, and then diluted to the mark. Appropriate amounts of solutions were taken and analyzed by DPV method.

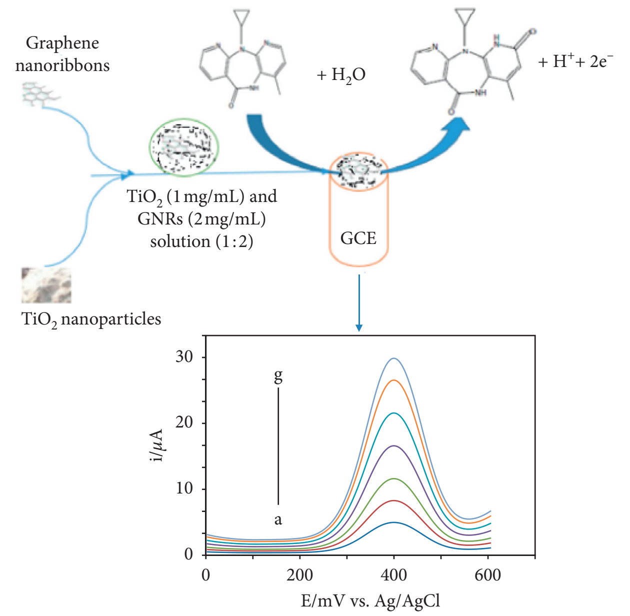

Scheme 1: The fabrication procedure of the electrochemical sensor.

3. Results and Discussion

3.1. Characterization. FT-IR spectra of TiO_2, GNR, and TiO_2/GNR composite are shown in Figure 1(a). The characteristic peaks in (b) were assigned as follows: 1654 cm^{-1} attributed to the stretching vibrations of carboxyl (-COOH) and at 1130 cm^{-1} corresponding to C-O-H bending and C-OH. The presence of such peaks can be used to explain the hybrid structure of graphene nanoribbons. After making the composite, the small peaks observed in (a) disappeared and peak intensity of C = O in GNR/TiO_2 shows some changes as a result of incorporation of nanoparticles (Figure 1(c)). The wavenumber region 3400 cm^{-1} is the stretching vibration of the hydroxyl group in all spectra. The morphology of prepared materials was observed using SEM (Figure 1(b)). As shown in Figure 1(a) TiO_2 nanospheres are aggregated in larger agglomerates. Figure 2(b) shows long curved rod-like structures of GNR [26]. The TiO_2 structures can be seen to be closely and homogeneously grown on the GNR (Figure 2(c)). For comparison, the GCE was included (Figure 1(d)).

EIS studies were done in the $[Fe(CN)_6]^{3-/4-}$ redox system to deduce the resistance to electron transfer. Nyquist plots (Figure 2) are shown by semicircle portions at high frequencies, while diffusion-limiting steps of the electrochemical process are shown by linear parts at lower frequencies. The equivalent circuit model used to fit impedance data into R_{et} values is shown as inset in Figure 2. From Table 1, it can be seen that modification of the GCE showed lowering of R_{et} except for TiO_2 with a larger diameter (2.2 kΩ) suggesting that TiO_2 acted as an insulating layer and barrier [18]. The incorporation of GNRs significantly lowered R_{et} values of GCE by 33.3% and that of TiO_2 in composite by 77.8%. The order as deduced from impedance values is TiO_2/GCE > GCE > GNR/GCE > TiO_2/GNR/GCE. The changes in R_{et} suggested proper modification of modified electrodes; hence, the electrode based on TiO_2/GNR composite was used throughout the study.

CV involving modified electrodes was performed in 1 mM $[Fe(CN)_6]^{3-/4-}$ and 0.1 M KCl electrolyte at a scan rate of 100 mV/s (Figure 2(b)). Redox peaks were observed on all tested electrodes with different peak current (i_p) and change in peak potential separation (ΔE_P) (Table 1). The effect of different modifiers was shown by ΔE_P, with lower ΔE_P showing better electron transfer ability. After drop-casting TiO_2/GNR on surface of GCE, i_{pa}, increased i_{pc}, and reduced E_p were observed compared to i_{pa}, i_{pc}, and E_p of GCE. The observation is attributed to TiO_2/GNR particles offering a large surface and good conductivity. Furthermore, the GNR acted as a suitable pathway to shuttle electrons; hence, improved peak currents were displayed. TiO_2/GCE showed a sluggish electron transfer process. The electrodes gave peak potential differences with the following trend: TiO_2<GCE < GNR/GCE < TiO_2/GNR/GCE. The obtained results are in good agreement with R_{et} values obtained from EIS results (Figure 2(c)). To see the change in area of modified electrode, electrode surface area of the TiO_2/GNR/GCE was determined in 1 mM $K_3[Fe(CN)_6]^{3-/4-}$ by applying the Randles–Sevcik equation:

$$i_p = 2.69 \times 10^5 n^{(3/2)} A_{eff} C v^{(1/2)}, \quad (1)$$

where i_p is the peak current, n is the number of electrons transferred ($n = 1$) during the redox couple Fe (II)/Fe (III), $D$is the diffusion coefficient of the analyte in solution ($7.6 \times 10^{-6}\ cm^2\ s^{-1}$), C is the solution concentration in mol/cm^3, A_{eff} is the effective surface area, and v is the scan rate (V/s). Voltammograms at different scan rates (50–300 mV/s) were run and gave a linear plot for $i_p versus v^{1/2}$. From the slope, TiO_2/GNR/GCE had an effective surface area of 0.208 cm^2 relative to the GCE area of 0.0712 cm^2 [27].

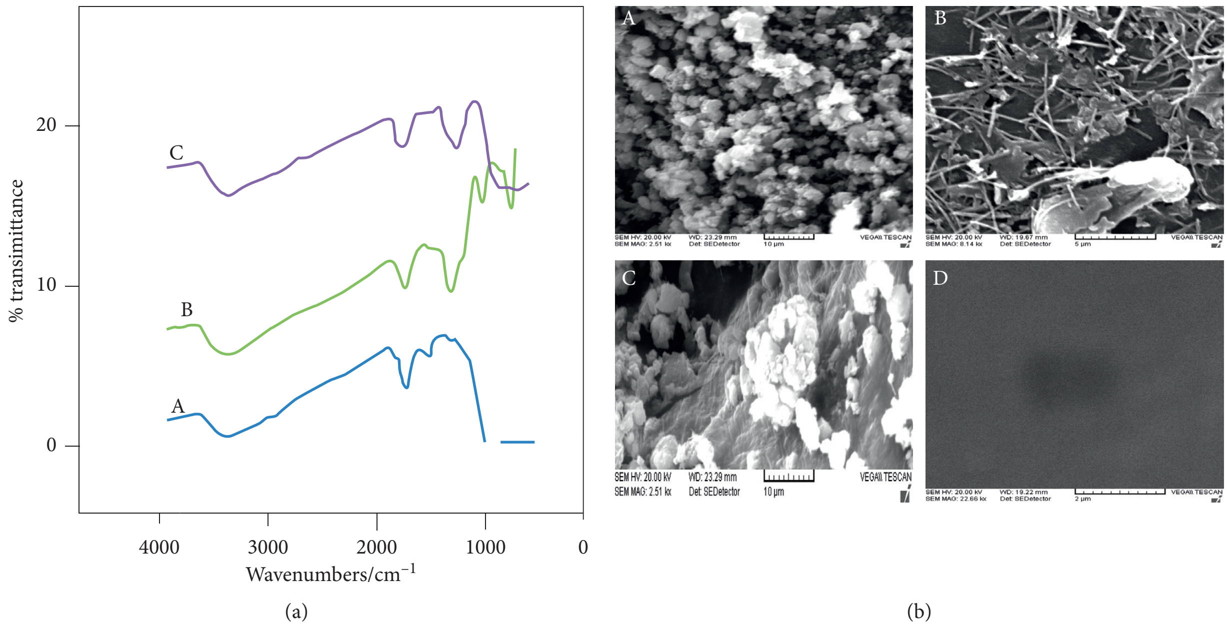

Figure 1: (a) FT-IR; (b) SEM images for (a) TiO_2 and (b) GNR; (c) TiO_2/GNR nanocomposite; (d) GCE.

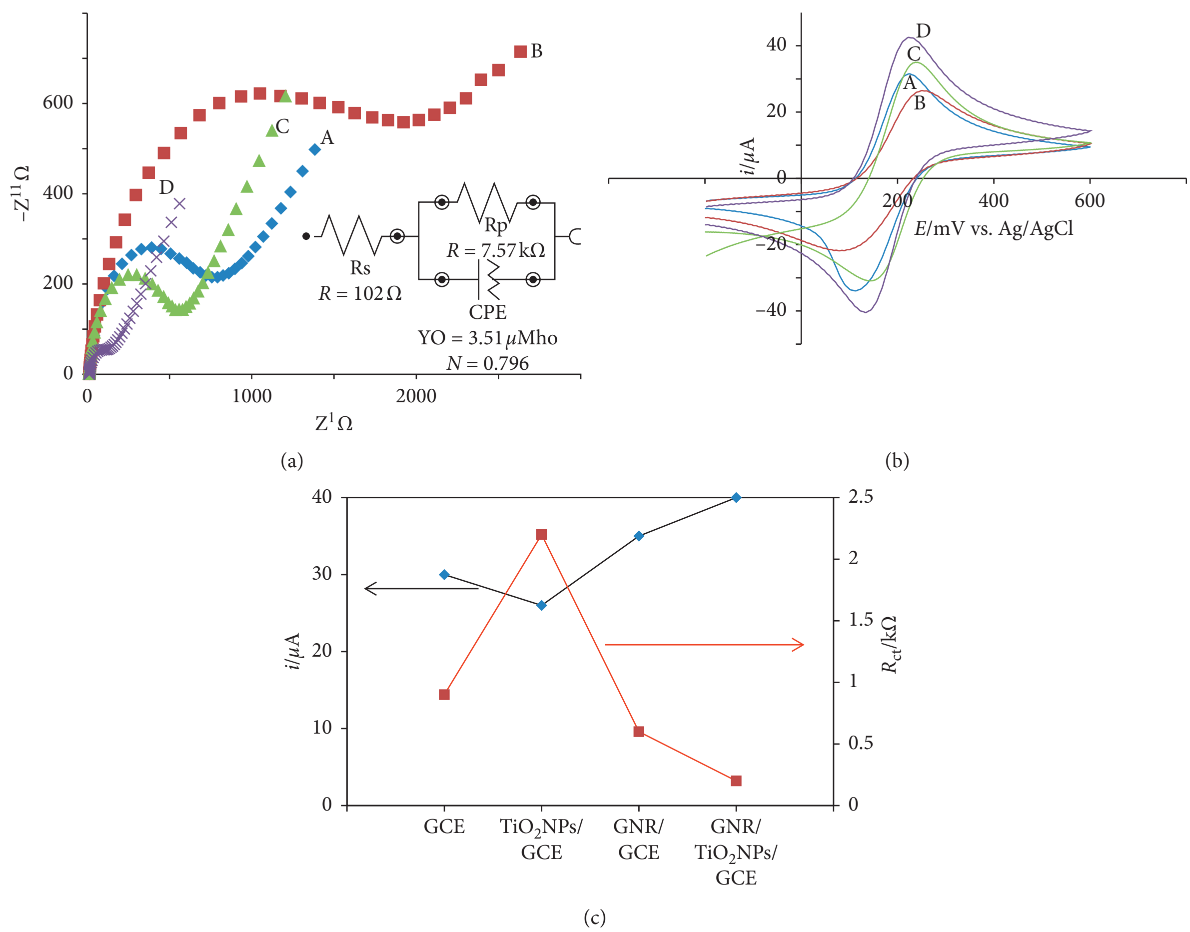

Figure 2: (a) EIS behavior of modified GCE in the presence of 1 mM $[Fe(CN)_6]^{3-/4-}$ in 0.1 M KCl; (b) CVs of the modified GCE in the presence of 1 mM $[Fe(CN)_6]^{3-/4-}$ in 0.1 M KCl at a scan rate of 100 mV s^{-1}. (c) Plot of i_{pa} and R_{et} *versus* modified GCEs; (a) GCE, (b) TiO_2/GCE, (c) GNR/GCE, and (d) TiO_2/GNR/GCE.

Table 1: Parameters for modified electrodes.

Electrodes	R_{et}/kΩ $[Fe(CN)_6]^{3-/4-}$ (0.1 M KCl)	ΔE_P $[Fe(CN)_6]^{3-/4-}$ (0.1 M KCl)	Nevirapine detection current (i_{pa}, μA)	Nevirapine detection potential (E_{pa}, mV)
GCE	0.9	100	6.6	742
TiO_2	2.2	120	14.0	779
GNR	0.6	85	14.4	490
TiO_2/GNR	0.20	83	18.9	390

3.2. Effect of pH. The electrochemical reaction of a biomolecule is usually affected by pH; hence, influence of pH on i_{pa} and E_{pa} was examined by cyclic voltammetry in the pH range of 7–12 in phosphate-buffered solutions at 100 mV/s (Figure 3). From the voltammograms in Figure 3, it can be seen that increasing pH results in biomolecule being easily oxidized, causing peak current and peak sharpness to increase as well. It should be noted that voltammograms in acidic media were not included, since no oxidation could be observed as a result of protonation on biomolecule. The repulsive forces between the biomolecule and the electrode surface of TiO_2/GNR/GCE slowed down arrival of biomolecules to the surface. As depicted in the inset, the current increases up to maximum of pH 11 and then decreases. Therefore, pH 11 was chosen as optimum pH for further studies. The peak potential was affected by pH as shown in the inset (Figure 3). The E_{pa} values of nevirapine were shifted to less positive values with increasing pH, showing deprotonation in the oxidation process at higher pHs [18]. A linear relationship was observed between E_{pa} and pH for the biomolecule with the following regression equations:

E_{pa} (mV) = −63.9 pH + 1123; $R^2 = 0.9508$ for nevirapine.

The slope for nevirapine (63.9 mV per pH)≈59.6 mV per pH indicates involvement of equal number of protons and electrons during oxidation reactions. This is in agreement with previous reports [5, 6, 28].

3.3. Cyclic Voltammetry Behavior of Nevirapine. It is pertinent to study the behavior of modified electrodes in PBS alone before any determinations (Figure 4(a)).

There was an increase in the peak background corrected current from GCE to TiO_2/GNR/GCE.

Graphene nanoribbons assisted in faster electron transport as well as providing a large surface area compared to TiO_2 alone. The electrochemical oxidation behavior of nevirapine was investigated by CV in 0.1 M PBS (pH 11.0) at modified electrodes (Figure 4(b)). The obtained voltammograms indicated electroactiveness of the compound and irreversible behavior. As shown in Figure 4(b), i_{pa} increased for nevirapine following modification on GCE; TiO_2/GCE < GNR/GCE < TiO_2/GNR (Table 1). The GCE exhibits very low i_{pa} at different potentials, whereas with the TiO_2 modified glassy carbon electrode under same conditions, i_{pa} increases compared to that of GCE (Figure 4(b)). On the other hand, when GNR was deposited on GCE, i_{pa} of nevirapine was found to be 2.2 times greater compared to GCE (Figure 4(c)). This may be attributed to fast electron transfer as well as high surface area available on the GNR for electrooxidation of nevirapine. The electrocatalytic oxidation of nevirapine with TiO_2/GNR composite modified GCE showed improved behaviors. An increase of i_{pa}, 186% for nevirapine, was deduced (Figure 4(d)), accompanied with a decrease in overpotential (352 mV) compared to glassy carbon electrode. The decrease in overpotential is caused by the synergetic effect of GNRs and TiO_2. TiO_2 nanoparticles help in electrocatalytic oxidation, whereas the GNRs provide larger surface area for TiO_2 as well as for nevirapine and then allow faster electrode kinetics. Hence, the TiO_2/GNR/GCE was used for the determination of nevirapine in the presence of interferent glucose in 0.1 M PBS (pH 11.0) using CV (Figure 4(c)). CV shows that it is possible for the biomolecules to be determined simultaneously with no overlap as shown by ΔE_{pa} of 410 mV.

In order to study nature of the electrode process, the influence of scan rate (ν) on i_{pa} and E_{pa} for a mixture of 0.1 mM glucose (interferent) and nevirapine in a 0.1 M PBS (pH 11.0) was examined by CV with scan rate ranging from 50 to 400 mV/s (Figure 5). From Figure 5 inset (a, b), i_{pa} is directly proportional to scan rate (ν) with a correlation coefficient of 0.9991 (nevirapine) and 0.9948 (glucose) showing electrochemical behavior of biomolecules on TiO_2/GNR modified electrode as adsorption controlled processes [4, 29, 30]. The adsorption mechanism process has also been reported for nevirapine [5, 6]. The presence of functional groups at edges of GNR in the composite might have facilitated adsorption of nevirapine by π–π stacking, hydrogen bonding, and covalent interactions [31]. Furthermore, plot of log i_{pa} against log ν (Figure 5(c), inset) gave a linear plot with the following equation:

log i_{pa} (μA) = 0.804 log ν (mV/s) + 0.493 for nevirapine.

The slope of nevirapine (0.804) is greater than the theoretical value of 0.5 V/s, which further confirms that electrochemical oxidation exhibits mixed behavior [32]. Additionally, from voltammograms, both biomolecules show i_{pa} increasing and E_{pa} shifting in the less positive value with increase in scan rate. The obtained results depict a totally irreversible electrochemical process.

3.4. Catalytic Rate Constants. Catalytic rate constants for nevirapine at TiO_2/GNR/GCE (Figure 6) were determined by chronoamperometry based on favorable oxidation results from voltammetry. The rate constants were evaluated using the following equation [33]:

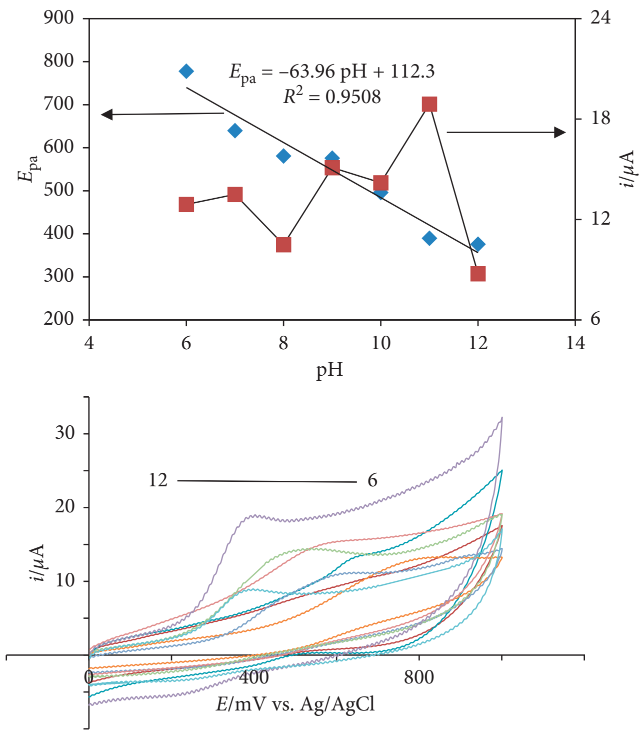

FIGURE 3: CVs for pH studies using TiO_2/GNR/GCE for nevirapine in 0.1 M PBS; 100 mV/s. Insets: plots of I_{pa} and E_{pa} *versus* pH.

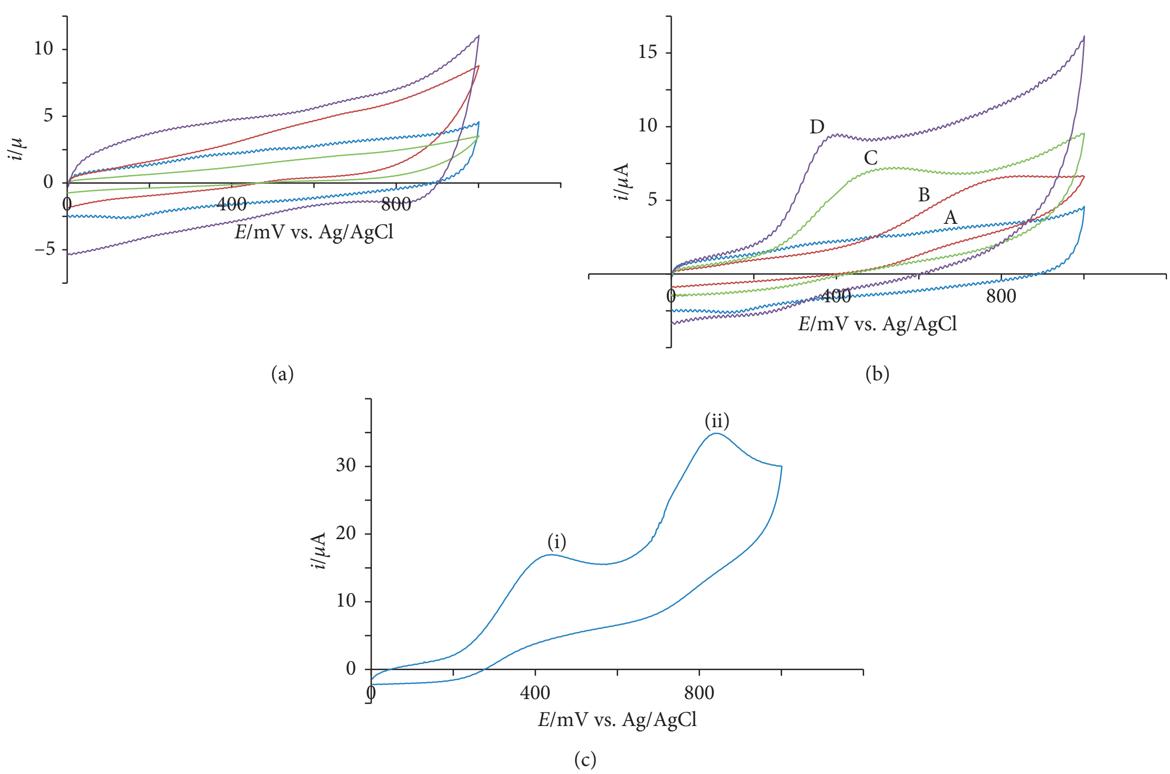

FIGURE 4: CVs in (a) 0.1 M PBS alone and (b) 1 mM nevirapine in 0.1 M PBS (pH 11.0): (a) GCE, (b) TiO_2/GCE, (c) GNR/GCE, and (d) TiO_2/GNR/GCE. (c) Simultaneous analysis of nevirapine and glucose at TiO_2/GNR/GCE, at a scan rate of 100 mV/s.

$$\frac{I_{cat}}{I_{buf}} = \frac{\gamma^{(1/2)}\left(\pi^{(1/2)}\operatorname{erf}\left(\gamma^{(1/2)}\right) + \exp^{-\gamma}\right)}{\gamma^{(1/2)}}, \tag{2}$$

where I_{cat} and I_{buf} are currents on TiO_2/GNR/GCE in presence and absence of nevirapine, respectively, $\gamma = kC_o t$ (C_o is the bulk concentration of nevirapine), and erf is the

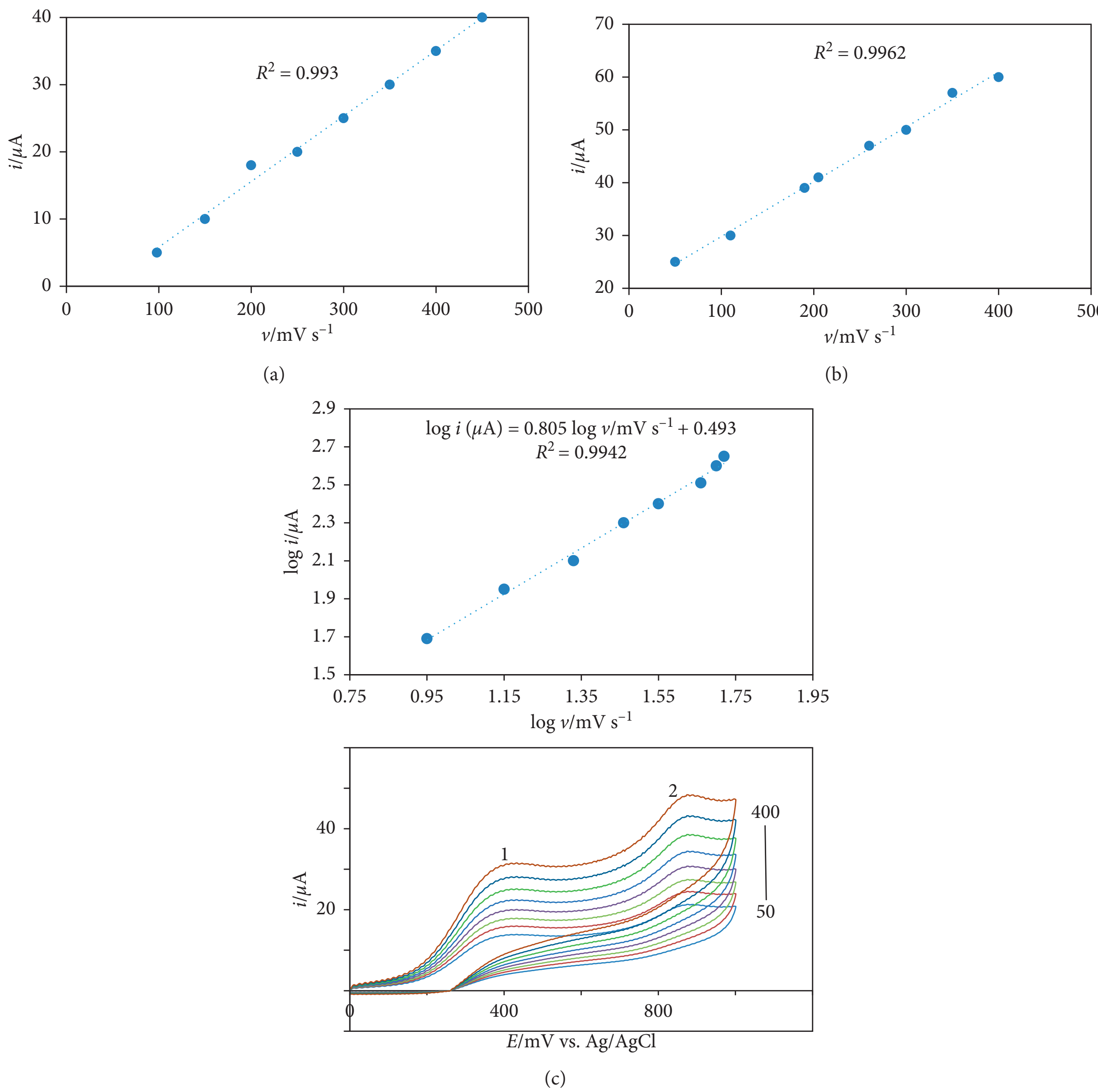

Figure 5: CVs of 0.1 mM nevirapine (1) and 0.1 mM glucose (2) in 0.1 M PBS (pH 11.0) at TiO_2/GNR/GCE (d) at various scan rates (50–400 mV/s). Inset: (a) plot i_{pa} (μA) *versus* v(mV/s); (b) log i_{pa} (μA) *versus* log v (mV/s) (nevirapine); (c) plot i_{pa} (μA) *versusv* (mV/s) (glucose).

error function. The error function is almost equal to 1 when γ exceeds 2 and hence equation (2) reduces to the following equation:

$$\frac{I_{cat}}{I_{buf}} = \gamma^{(1/2)}\pi^{(1/2)} = \pi^{(1/2)}\left(kC_o\ t\right)^{(1/2)}, \qquad (3)$$

where k is the catalytic rate constant (cm^3/mol/s) and t is the time elapsed in (s). The catalytic rate constants for nevirapine were calculated based on information obtained from chronoamperometry (Figure 6). A plot of I_{cat}/I_{buf} versus $t^{1/2}$ for oxidation of nevirapine gave a linear plot. The calculated values of catalytic constants were $7.9 \times 10^5\ cm^3$/mol/s. The calculated values further elucidate sharp features of catalytic i_{pa} of nevirapine at the surface of TiO_2/GNR/GCE.

3.5. Nevirapine Determination by Differential Pulse Voltammetry. Determination of nevirapine in the absence of interferents was investigated (Figure 7(a)). In all cases, i_{pa} increased with increase in concentration of analyte as shown by voltammograms and the analytical parameters shown in Table 2.

3.6. Behavior of Nevirapine in the Presence of Interferent. The effect of different concentrations of analyte on electrochemical response of nevirapine and interferent glucose on TiO_2/GNR modified electrode was investigated (Figures 8(a)–8(c)). Different cases were studied, where the concentration of only one compound was varied, while the concentration of the other compound was kept constant. In the first case, the concentration of nevirapine was changed,

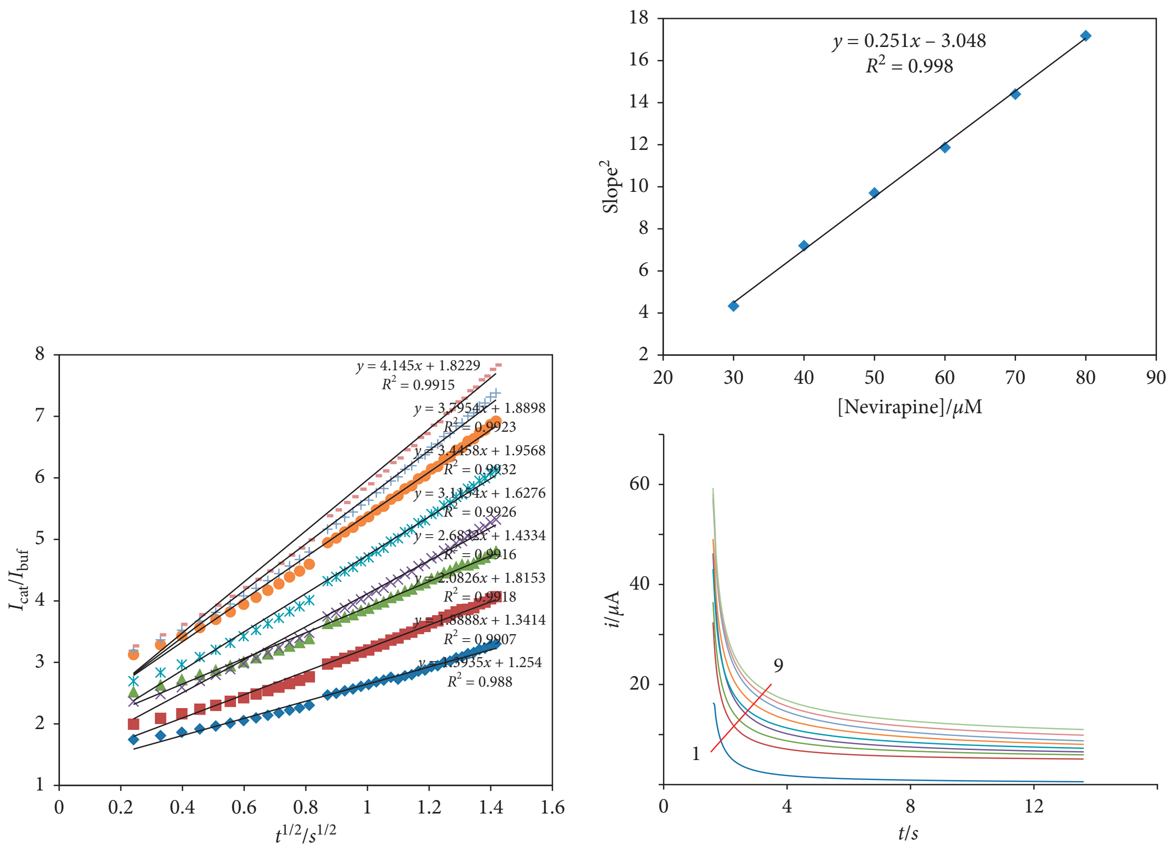

(a) (b)

Figure 6: Chronoamperograms for different nevirapine concentrations in 0.1 M PBS (pH 11), curves 2–9 : 0.1–0.7 μM. Insets: (a) plots of i_{cat}/i_{buffer} versus $t^{1/2}$; (b) Slope^2*versus* [nevirapine].

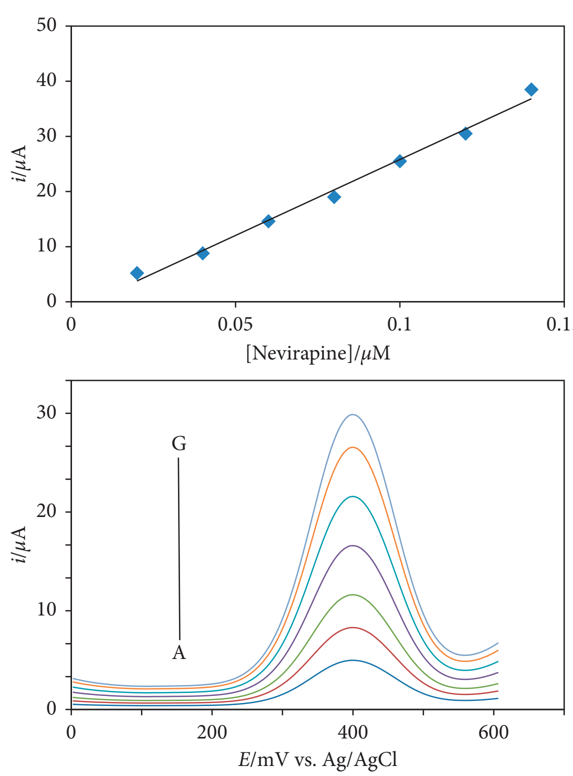

Figure 7: DPVs of TiO_2/GNR/GCE in different concentrations of nevirapine. *Inset* plot of i_{pa} (μA) *versus* [nevirapine]/μM in 0.1 M PBS solution, pH 11.0.

Table 2: Analytical parameters for electrochemical determination of nevirapine in 0.1 M PBS at pH 11.0.

Analyte	E(mV)	LDR (μM)	Linear regression equation (y ↔ i/μA; x ↔ [analyte], μM)	R^2	LOD (μM)	RSD (%)
Nevirapine[a]	+400	0.020–0.14	$y = 25.36\ x + 1.73$	0.9912	0.041	2.65
Glucose[b]	+800	0.020–0.14	$y = 321.43x + 7.94$	0.9914	0.012	1.42
Nevirapine[b]	+400	0.020–0.14	$y = 269.52x + 1.13$	0.9872	0.043	2.60
Glucose[c]	+800	0.020–0.14	$y = 402.91x + 6.12$	0.9971	0.012	1.48
Nevirapine[c]	+400	0.020–0.14	$y = 75.00x + 6.07$	0.9911	0.043	2.65
Nevirapine[d]	–	Log (0.20–1.2)	R_{et} (kΩ) = −2.28 log x + 1.06	0.9842	0.070	2. 75

[a]Statistical data for DPV single analyte determination. [b]Statistical data from DPV for single analyte when the concentration of the other analyte is kept constant. [c]Statistical data from DPV for both analytes simultaneously determined. [d]Impedimetric determination.

while the concentration of glucose was kept constant (Figure 8(a)). As shown in Figure 8(a), DPP was obtained with different concentrations (0.20–1.4 μM) of nevirapine in presence of 0.20 μM glucose on TiO_2/GNR modified electrode. The oxidation peak currents increased linearly when the bulk concentration of nevirapine was also increased. Furthermore, the oxidation peak currents of glucose remained the same as the numbers of cycles were increased. The inset (Figure 8(a)) shows a plot of i_{pa}*versus* different concentrations of nevirapine.

On the other hand, Figure 8(b) shows DPVs obtained in different concentrations (0.20–1.4 μM) of glucose in presence of 0.20 μM nevirapine. The same trend was observed with the glucose molecule, where i_{pa} corresponding to oxidation of glucose showed linearity with an increase in the bulk concentration of glucose, and i_{pa} for the oxidation of nevirapine remained the same as the number of cycles increased. A plot of i_{pa}*versus* different concentrations of glucose is shown as inset (Figure 8(b)). The analytical parameters are shown in Table 2. Figure 8(c) shows DPVs obtained at TiO_2/GNR modified electrode when equal concentrations of nevirapine and glucose were simultaneously changed. As shown in Figure 8(c), clearly resolved voltammetric signals were observed for addition of increasing concentrations with calibration curves as insets. The analytical parameters of the calibration plots are listed in Table 2. From the use of TiO_2/GNR modified electrode, it is interesting to note the detection of glucose and nevirapine is independent as shown by detection limits and clear peak potential separation. A comparison of the detection limits of the present method with those reported in recent years at other surfaces is tabulated in Table 3. The values of limit of detection (LOD) were calculated using $3s/k$ (where s is the standard deviation of the blank and k is the slope of the calibration curve) and using Figures 7, 8(a)–8(c), and 9. It can be clearly seen that the LOD observed using TiO_2/GNR is much lower. The synergic effects between TiO_2 and excellent physicochemical properties of GNR make the composite highly suitable for nevirapine and glucose sensing.

3.7. Impedimetric Determination. EIS was also employed to study the oxidation behavior of nevirapine at TiO_2/GNR/GCE (Figure 9(a)). The results showed that, in absence of nevirapine, Nyquist diagram comprises a large semicircle at high frequencies due to large charge transfer resistance (2.5 kΩ). In the presence of interferent glucose and biomolecule nevirapine, diameter of the semicircle decreases, confirming the electrocatalytic capability of composite. However, glucose showed a smaller R_{et} value of 0.5 kΩ, while nevirapine had a large value of 0.75 kΩ. The lower R_{et} in glucose showed that TiO_2/GNR provided more favorable orientation and conductive pathway for transfer of electrons. Overall, it can be concluded that TiO_2/GNR sensor was specific towards oxidation of glucose and nevirapine.

The EIS responses of fabricated sensors to different concentrations of nevirapine were carried out further (Figure 9(b)). It can be seen in Figure 9(a) that R_{et} decreased with increasing nevirapine concentration. The observations can be attributed to TiO_2/GNR offering a suitable platform for oxidation of the biomolecule. Increasing the concentrations of biomolecule, as shown Figure 9(b), results in generation of more electrons (nevirapine $2e^-$), causing R_{et} values to decrease markedly, consequently enhancing the electrode kinetics. Under the optimized conditions, the electrochemical sensor gave parameters as shown in Table 2. The LODs are comparable to both single detections of analytes when one is constant and in equal concentrations of the analytes. The results obtained clearly elucidate possible impedimetric detection of nevirapine using GNR and TiO_2 in the composite.

3.8. Other Interferent Ions. For demonstrating selectivity of TiO_2/GNR/GCE, EIS was obtained before and after interactions with each interferent and values for ΔR_{et} were obtained as $R_{et}(\text{after interaction}) - R_{et}(\text{before interaction})$. The fabricated sensor was incubated in the presence of some interferent ions such as Na^+, K^+, Cl^-, Ca^{2+}, Mg^{2+}, and PO_4^{3-} and possible biomolecules (sucrose, ascorbic acid, dopamine, tyrosine, glycine, uric acid, lopinavir, stavudine, zidovudine, lamivudine, and efavirenz) to a solution containing nevirapine (0.2 μM). It should be noted that biomolecules that normally coexist with nevirapine were selected. From the Nyquist plots, the results showed that 200-fold excess of Na^+, K^+, Ca^{2+}, Mg^{2+}, PO_4^{3-}, Cl^-, and sucrose and 100-fold excess of glycine, tyrosine, and uric acid showed no major influences on changes in R_{et}. For nevirapine alone, negligible changes in R_{et} in the presence of lopinavir, stavudine, zidovudine, lamivudine, and efavirenz were observed. By looking at all obtained small values of ΔR_{et}, practical applicability of proposed electrode for determination of nevirapine is possible. Similar results have been reported in literature based on different methods [3, 6].

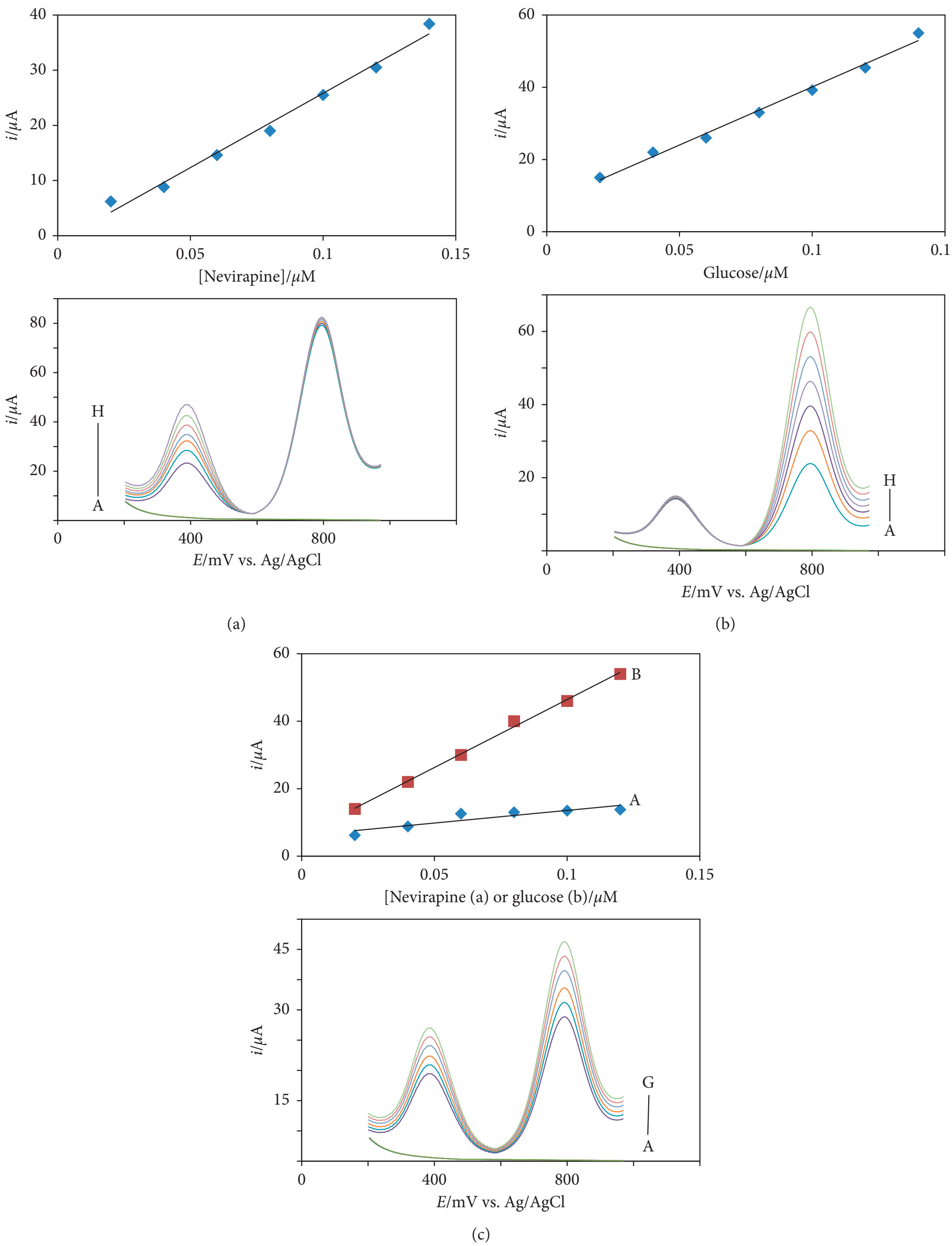

FIGURE 8: DPVs of TiO_2/GNR/GCE for (a) 0.2 μM glucose (kept constant) and different concentrations of nevirapine. *Inset* plot of i_{pa} (μA) *versus* [nevirapine]/μM; (b) 0.2 μM nevirapine (kept constant) and different concentrations of glucose. *Inset*: plot of i_{pa} (μA) *versus* [glucose]/μM; (c) DPV for different concentrations of nevirapine and glucose, all in 0.1 M PBS solution, pH 11.0. Different concentrations ranged from 0.02 to 0.14 μM.

Table 3: A comparison of analysis results of nevirapine at TiO_2/GNR sensor with recently reported sensors.

Modifier	Analysis technique	Electrolyte type, pH	Type of analysis	LOD (μM)	LR (μM)	Reference
AuNPs/p (MB)/f-MWCNTs/GE)	DPASV	PBS, 11	Single	53	0.1–50	[6]
CuO-CNP-GCE	LSV	BR buffer 7	Single	66	0.1–100	[3]
Ura/CPE	DPV	0.1 M NaOH, 13	Single	0.05	0.1–70	[1]
CP-Bi_2O_3	DPV	PBS, 8	Single	0.110	0.05–50	[29]
Pd@rGO/MoS_2 QDs	DPV	PBS, 10	Single	0.05	0.1–80	34
TiO_2/GNR	DPV	PBS, 11	Simultaneous	0.043	0.020–0.14	Present work

Au NPs, gold nanoparticles; DPASV, differential pulse anodic stripping voltammetry, Ura/CPE, uracil-modified carbon paste electrode; CuO-CNP-GCE, copper oxide carbon nanoparticles glassy carbon electrode; LSV, linear sweep voltammetry; CP-Bi_2O_3, carbon paste electrode modified with Bi_2O_3.

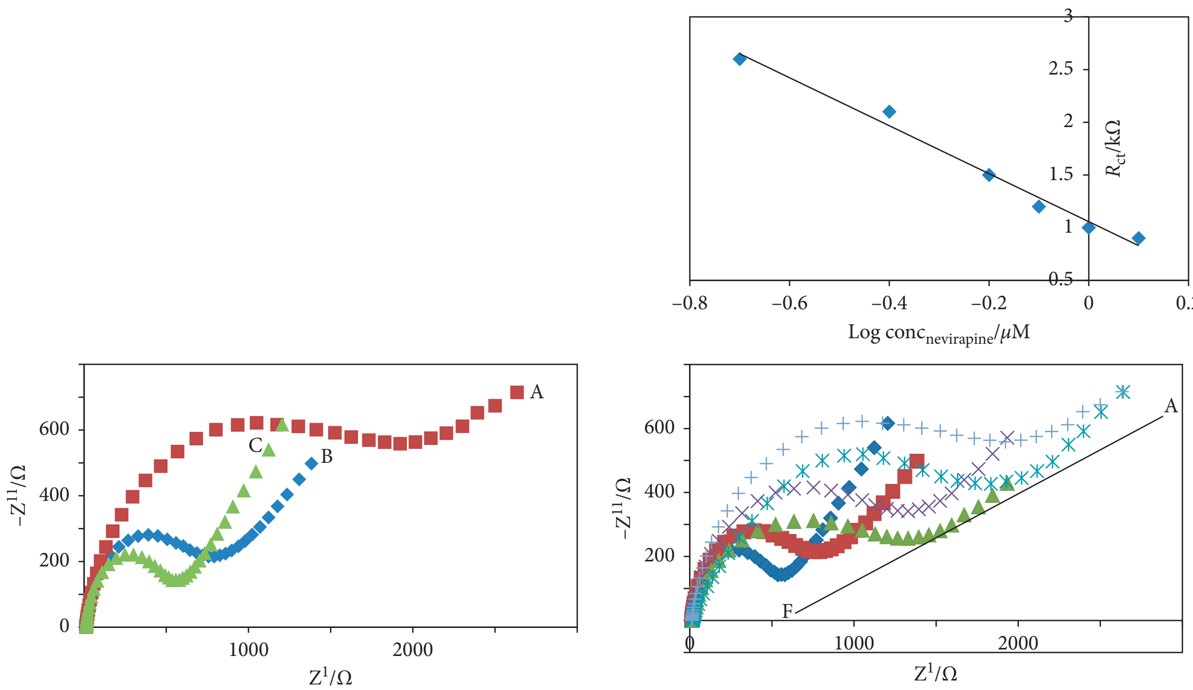

(a) (b)

Figure 9: Nyquist diagrams of TiO_2/GNR/GCE (a) in the absence (a) and in the presence of 0.2 μM nevirapine and (b) in the presence of 0.2 μM glucose (c). Different concentrations of (b) nevirapine in 0.1 M PBS (pH 11.0). Insets: calibration plots.

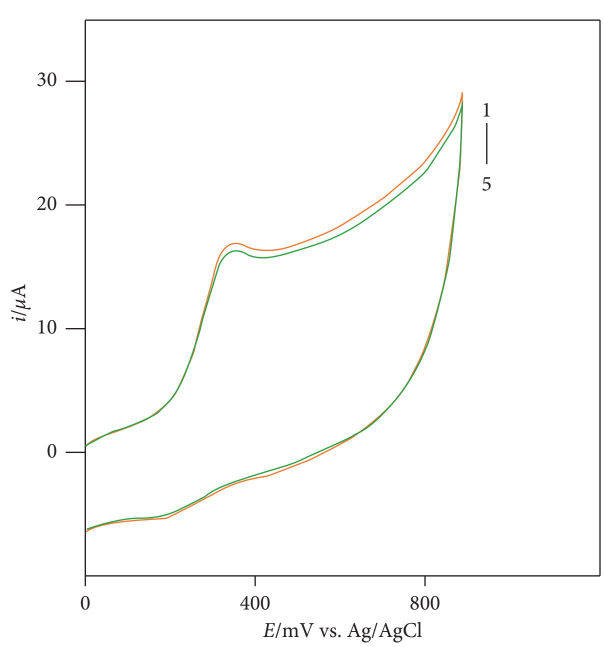

Figure 10: CVs for 0.1 mM nevirapine obtained after 5 test runs. Scan rate = 100 mV/s in PBS (pH 11).

Table 4: Results of analysis of nevirapine in pharmaceutical formulations by the DPV method.

	Nevirapine
Labelled amount (mg)	200
Amount found (mg)	198.5 ± 0.20
Recovery (%)	99.25
Pure nevirapine added to tablet solution (mg)	15
Amount found (mg)	15.12 ± 0.01
Recovery (%)	100.8

3.9. Reproducibility Studies. When developing sensors, reproducibility is a significant process to be investigated. The TiO_2/GNR sensor was investigated through five repetitive measurements of 0.1 mM of nevirapine in PBS (pH 11) by CV (Figure 10). The relative standard deviation of i_{pa} responses to nevirapine sensing was less than 3.5%, indicating good reproducibility.

3.10. Nevirapine in Pharmaceutical Formulations. The results obtained from the developed sensor for determining amount of nevirapine in commercially available tablets are shown in Table 4. These were calculated after running working solutions prepared after suitable dilution with DPV. The results of analysis were found to be satisfactory as shown by high recovery values.

4. Conclusions

A selective nevirapine electrochemical sensor was developed based on the modification of a GCE with metal oxide and graphene nanoribbons nanocomposite. The successful preparation of GNR and TiO_2 was confirmed by FT-IR and SEM. EIS confirmed superior electrochemical properties of the prepared TiO_2/GNR/GCE in comparison to bare GCE. It was also illustrated that TiO_2/GNR/GCE offered a low potential during detection by cyclic voltammetry. The obtained TiO_2/GNR/GCE composite exhibited good reproducibility during analysis. The developed method was successfully applied to the quantification of nevirapine in a pharmaceutical formulation. The present study provides a general strategy for monitoring drug-food behavior during electrochemical applications.

Data Availability

Data will be shared through the authors' library repository if accepted.

Conflicts of Interest

The authors declare that there are no conflicts of interest regarding the publication of this paper.

References

[1] F. Zhang, L. Li, L. Luo, Y. Ding, and X. Liu, "Electrochemical oxidation and determination of antiretroviral drug nevirapine based on uracil-modified carbon paste electrode," *Journal of Applied Electrochemistry*, vol. 43, no. 3, pp. 263–269, 2013.

[2] W. Chen, W. Li, X. Ling, X. Wang, and J. Liu, "Study on the interaction between HIV reverse transcriptase and its non-nucleoside inhibitor nevirapine by capillary electrophoresis," *Journal of Chromatography B*, vol. 878, no. 20, pp. 1714–1717, 2010.

[3] S. Shahrokhian, R. Kohansal, M. Ghalkhani, and M. K. Amini, "Electrodeposition of copper oxide nanoparticles on pre-casted carbon nanoparticles film for electrochemical investigation of anti-HIV drug nevirapine," *Electroanalysis*, vol. 27, no. 8, pp. 1989–1997, 2015.

[4] R. M. Lopez, L. Pou, M. R. Gomez, I. Ruiz, and J. Monterde, "Simple and rapid determination of nevirapine in human serum by reversed-phase high-performance liquid chromatography," *Journal of Chromatography B: Biomedical Sciences and Applications*, vol. 751, no. 2, pp. 371–376, 2001.

[5] M. Moyo, J. O. Okonkwo, and N. M. Agyei, "An amperometric biosensor based on horseradish peroxidase immobilized onto maize tassel-multi-walled carbon nanotubes modified glassy carbon electrode for determination of heavy metal ions in aqueous solution," *Enzyme and Microbial Technology*, vol. 56, pp. 28–34, 2014.

[6] M. B. Gholivand, E. Ahmadi, and M. Haseli, "A novel voltammetric sensor for nevirapine, based on modified graphite electrode by MWCNs/poly (methylene blue)/gold nanoparticle," *Analytical Biochemistry*, vol. 527, pp. 4–12, 2017.

[7] M. Ghalkhani and S. Shahrokhian, "Application of carbon nanoparticle/chitosan modified electrode for the square-wave adsorptive anodic striping voltammetric determination of Niclosamide," *Electrochemistry Communications*, vol. 12, no. 1, pp. 66–69, 2010.

[8] Y. Oztekin, Z. Yazicigil, A. Ramanaviciene, and A. Ramanavicius, "Polyphenol-modified glassy carbon electrodes for copper detection," *Sensors and Actuators B: Chemical*, vol. 152, no. 1, pp. 37–48, 2011.

[9] M. Raj and R. N. Goyal, "Graphene nanoribbons/poly-bromocresol green based sensor for the simultaneous determination of 3,4-dihydroxyphenylacetic acid and 5-hydroxyindoleacetic acid," *Journal of The Electrochemical Society*, vol. 164, no. 13, pp. B695–B703, 2017.

[10] R. D. Tandel, R. S. Naik, and J. Seetharamappa, "Electrochemical characteristics and electrosensing of an antiviral drug, entecavir via synergic effect of graphene oxide nanoribbons and ceria nanorods," *Electroanalysis*, vol. 29, pp. 1–10, 2017.

[11] X. Jia, J. Campos-Delgado, M. Terrones, V. Meunier, and M. S. Dresselhaus, "Graphene edges: a review of their fabrication and characterization," *Nanoscale*, vol. 3, no. 1, pp. 86–95, 2011.

[12] T. Shimizu, J. Haruyama, D. C. Marcano et al., "Large intrinsic energy bandgaps in annealed nanotube-derived graphene nanoribbons," *Nature Nanotechnology*, vol. 6, no. 1, pp. 45–50, 2011.

[13] J. Lin, Z. Peng, C. Xiang et al., "Graphene nanoribbon and nanostructured SnO2 composite anodes for lithium ion batteries," *ACS Nano*, vol. 7, no. 7, pp. 6001–6006, 2013.

[14] D. Krepel, J. E. Peralta, G. E. Scuseria, and O. Hod, "Graphene nanoribbons-based ultrasensitive chemical detectors," *The Journal of Physical Chemistry C*, vol. 120, no. 7, pp. 3791–3797, 2016.

[15] U. Rajaji, R. Arumugam, S.-M. Chen et al., "Graphene nanoribbons in electrochemical sensors and biosensors: a review," *International Journal of Electrochemical Science*, vol. 13, pp. 6643–6654, 2018.

[16] D. Wang, X. Li, J. Yang et al., "Hierarchical nanostructured core-shell Sn@C nanoparticles embedded in graphene

nanosheets: spectroscopic view and their application in lithium ion batteries," *Physical Chemistry Chemical Physics*, vol. 15, no. 10, pp. 3535–3542, 2013.

[17] P. T. Mafuwe, M. Moyo, T. Mugadza, M. Shumba, and S. Nyoni, "Cobalt oxide nanoparticles anchored polyaniline-appended cobalt tetracarboxy phthalocyanine, modified glassy carbon electrode for facile electrocatalysis of amitrole," *Journal of Solid State Electrochemistry*, vol. 23, no. 1, pp. 285–294, 2019.

[18] M. Moyo, P. Mudarikwa, M. Shumba, and J. O. Okonkwo, "Voltammetric sensing of nitrite in aqueous solution using titanium dioxide anchored multiwalled carbon nanotubes," *Ionics*, vol. 24, no. 8, pp. 2489–2498, 2018.

[19] R. Jain and Dhanjai, "TiO_2-multi walled carbon nanotubes hybrid film sensor for sensing of antiprotozoal agent satranidazole in solubilized system," *Journal of ElectrochemicalSociety*, vol. 160, no. 8, pp. H474–H480, 2013.

[20] Y. Fan, J.-H. Liu, H.-T. Lu, and Q. Zhang, "Electrochemical behavior and voltammetric determination of paracetamol on Nafion/TiO2-graphene modified glassy carbon electrode," *Colloids and Surfaces B: Biointerfaces*, vol. 85, no. 2, pp. 289–292, 2011.

[21] J.-Y. Sun, K.-J. Huang, S.-F. Zhao, Y. Fan, and Z.-W. Wu, "Direct electrochemistry and electrocatalysis of hemoglobin on chitosan-room temperature ionic liquid-TiO2-graphene nanocomposite film modified electrode," *Bioelectrochemistry*, vol. 82, no. 2, pp. 125–130, 2011.

[22] A. Kumaravel and M. Chandrasekaran, "A biocompatible nano TiO2/nafion composite modified glassy carbon electrode for the detection of fenitrothion," *Journal of Electroanalytical Chemistry*, vol. 650, no. 2, pp. 163–170, 2011.

[23] M. Hasanzadeh, A. Karimzadeh, N. Shadjou et al., "Graphene quantum dots decorated with magnetic nanoparticles: synthesis, electrodeposition, characterization and application as an electrochemical sensor towards determination of some amino acids at physiological pH," *Materials Science and Engineering: C*, vol. 68, pp. 814–830, 2016.

[24] V. Vukojević, S. Djurdjić, M. Ognjanović et al., "Enzymatic glucose biosensor based on manganese dioxide nanoparticles decorated on graphene nanoribbons," *Journal of Electroanalytical Chemistry*, vol. 823, pp. 610–616, 2018.

[25] R. Zhang, C.-L. Sun, Y.-J. Lu, and W. Chen, "Graphene nanoribbon-supported ptpd concave nanocubes for electrochemical detection of tnt with high sensitivity and selectivity," *Analytical Chemistry*, vol. 87, no. 24, pp. 12262–12269, 2015.

[26] D. V. Kosynkin, A. L. Higginbotham, A. Sinitskii et al., "Longitudinal unzipping of carbon nanotubes to form graphene nanoribbons," *Nature*, vol. 458, no. 7240, pp. 872–876, 2009.

[27] B. Xiao, X. Li, X. Li et al., "Graphene nanoribbons derived from the unzipping of carbon nanotubes: controlled synthesis and superior lithium storage performance," *The Journal of Physical Chemistry C*, vol. 118, no. 2, pp. 881–890, 2014.

[28] V. Usai, T. Mugadza, F. Chigondo et al., "Synthesis and characterisation of cobalt oxide nanoparticles decorated graphene oxide and its electrocatalytic behaviour," *Polyhedron*, vol. 157, pp. 192–199, 2019.

[29] N. L. Teradal and J. Seetharamappa, "Bulk modification of carbon paste electrode with Bi_2O_3 nanoparticles and its application as an electrochemical sensor for selective sensing of an ati-HIV drug nevirapine," *Electroanalysis*, vol. 27, pp. 2007–2016, 2007.

[30] N. P. Shetti, S. J. Malode, and S. T. Nandibewoor, "Electrochemical behavior of an antiviral drug acyclovir at fullerene-C60-modified glassy carbon electrode," *Bioelectrochemistry*, vol. 88, pp. 76–83, 2012.

[31] M. Tefera, A. Geto, M. Tessema, and S. Admassie, "Simultaneous determination of caffeine and paracetamol by square wave voltammetry at poly (4-amino-3-hydroxynaphthalene sulfonic acid)-modified glassy carbon electrode," *Food Chemistry*, vol. 210, pp. 156–162, 2016.

[32] A. Martín, J. Hernández-Ferrer, L. Vázquez, M.-T. Martínez, and A. Escarpa, "Controlled chemistry of tailored graphene nanoribbons for electrochemistry: a rational approach to optimizing molecule detection," *RSC Advances*, vol. 4, no. 1, pp. 132–139, 2014.

[33] J. A. Bard and R. L. Faulkner, *Electrochemical Methods*, pp. 503-504, Wiley, Hoboken, NJ, USA, 2001.